International Journal of Heat and Fluid Flow 29 (2008) 841–855

Contents lists available at ScienceDirect

International Journal of Heat and Fluid Flow

journal homepage: www.elsevier.com/locate/ijhff

# DNS and LES of estimation and control of transition in boundary layers subject to free-stream turbulence

Antonios Monokrousos *, Luca Brandt, Philipp Schlatter, Dan S. Henningson

*Linné Flow Centre, KTH Mechanics, Osquars Backe 18, SE-100 44 Stockholm, Sweden*

ARTICLE INFO

*Article history:*
Received 2 November 2007
Received in revised form 21 February 2008
Accepted 8 March 2008
Available online 5 May 2008

*Keywords:*
Boundary layer
Bypass transition
Optimal control
State estimation
Direct numerical simulation (DNS)
Large-eddy simulation (LES)

ABSTRACT

Transition to turbulence occurring in a flat-plate boundary-layer flow subjected to high levels of free-stream turbulence is considered. This scenario, denoted bypass transition, is characterised by the non-modal growth of streamwise elongated disturbances. These so-called streaks are regions of positive and negative streamwise velocity alternating in the spanwise direction inside the boundary layer. When they reach large enough amplitudes, breakdown into turbulent spots occurs via their secondary instability. In this work, the bypass-transition process is simulated using direct numerical simulations (DNS) and large-eddy simulations (LES). The ADM-RT subgrid-scale model turned out to be particularly suited for transitional flows after a thorough validation.

Linear feedback control is applied in order to reduce the perturbation energy and consequently delay transition. This case represents therefore an extension of the linear approach (Chevalier, M., Hoepffner, J., Åkervik, E., Henningson, D.S., 2007a. Linear feedback control and estimation applied to instabilities in spatially developing boundary layers. J. Fluid Mech. 588, 163–187, 167–187.) to flows characterised by strong nonlinearities. Control is applied by blowing and suction at the wall and it is both based on the full knowledge of the instantaneous velocity field (i.e. full information control) and on the velocity field estimated from wall measurements.

The results show that the control is able to delay the growth of the streaks in the region where it is active, which implies a delay of the whole transition process. The flow field can be estimated from wall measurements alone: The structures occurring in the "real" flow are reproduced correctly in the region where the measurements are taken. Downstream of this region the estimated field gradually diverges from the "real" flow, revealing the importance of the continuous excitation of the boundary layer by the external free-stream turbulence. Control based on estimation, termed compensator, is therefore less effective than full information control.



## 1. Introduction

The aim of this study is to perform numerical simulations to apply linear feedback control to transitional boundary-layer flows in the presence of free-stream turbulence where bypass transition occurs. An efficient pseudo-spectral numerical discretization is used and tools from modern control theory are incorporated into the controller design. Both large-eddy and direct numerical simulations are performed for evaluating the control efficiency in a highly nonlinear configuration.

### 1.1. Flow control

Control of wall-bounded transitional and turbulent flows is the object of the present investigation owing to the high potential benefits. Any reduction of the skin friction, for example, implies relevant savings of the operational cost of commercial aircrafts and cargo ships. In particular, the bypass transition scenario considered here is relevant in turbomachinery where high levels of free-stream turbulence are present.

Direct numerical simulations (DNS) have provided physical insight into the phenomena of transitional and turbulent flows, despite the fact that they are limited to simple and moderate Reynolds-number flows (Moin and Mahesh, 1998). The same tools are now adopted to investigate the feasibility and performance of feedback control algorithms on a complex transitional flow case.

A linear model-based feedback control approach, that minimises an objective function which measures the perturbation energy, is formulated where the Orr–Sommerfeld and Squire equations model the flow dynamics. The latter equations describe the linear evolution of perturbations evolving in a parallel base flow. The requirement implicit in this formulation is the need of complete state information. However, the control problem can be combined with

* Corresponding author.
*E-mail address:* antonios.monokrousos@mech.kth.se (A. Monokrousos).

0142-727X/$ - see front matter © 2008 Elsevier Inc. All rights reserved.
doi:10.1016/j.ijheatfluidflow.2008.03.009

a state estimator to relax this requirement. The information problem is a limiting factor in the success of a control scheme, since, as a first step, it affects the whole procedure. The so-called Kalman and the extended Kalman filter have been implemented in order to reconstruct the flow in an optimal manner by only considering wall measurements (Kailath and Hassibi, 2000).

Flow control has been the object of comprehensive investigation the past years and recently, much effort has been put in the combination of computational fluid dynamics and control theory. While early attempts of flow control were based on physical intuition or on a trial-and-error basis, more systematic approaches are now followed. General reviews on flow control can be found in Moin and Bewley (1994), Joslin et al. (1996), Bewley (2001) and Kim and Bewley (2007) to mention a few.

Different control strategies have been attempted over the years for transitional flows, for example, wave cancellation where Tollmien–Schlichting waves are damped by applying anti-phase signals. Early reviews on the subject can be found in Thomas (1990) and Metcalfe (1994). Wave-cancellation methods for control were applied already in the 1980s both experimentally (Thomas, 1983) and numerically, see e.g. Laurien and Kleiser (1989). A more 'drastic' control strategy, also known as laminar flow control, consists in stabilising the flow by applying strong suction on the boundary layer thus modifying the mean flow profile. A review on this method can be found in Joslin (1998). Nonlinear control methods have been studied as well and an overview of these methods is given by Joslin et al. (1997). In many cases, nonlinear control is applicable only within the conditions and parameter range that it is designed for. An example of a robust controller that addresses that problem is described by Bewley et al. (2000). Other examples of application of nonlinear controllers are Berggren (1998), Bewley et al. (2001) and Collis et al. (2000).

The use of linear feedback controllers has been investigated more recently. This was motivated by the understanding on how the energy growth of fluctuations in a turbulent flow is related to linear mechanisms. In particular, Farrell and Ioannou (1996), Henningson (1996) and Kim and Lim (2000) showed that linear mechanisms are important to sustain turbulence and thus linear controllers can be applied for turbulence control. One early work on linear feedback control schemes is Joshi et al. (1995). Results from the application of linear optimal control theory also confirm the importance of linear mechanisms in the nonlinear flows under consideration (Högberg and Henningson, 2002). Relaminarisation of turbulent channel flow was achieved by Högberg et al. (2003a) with this method and the controller and estimator were combined by Högberg et al. (2003b). The combined control and estimation problem is also known as a "compensator".

Recent studies from our group on the application of model-based linear feedback control have shown the importance of physically relevant stochastic models for the estimation problem which turns out to be crucial for fast convergence (Hoepffner et al., 2005; Chevalier et al., 2006). Such stochastic noise needs to describe accurately enough the unmodelled dynamics, like uncertainties and nonlinearities. Based on these models the estimator is shown to work for both infinitesimal as well as finite amplitude perturbations in numerical simulations. The compensator has been applied to spatially developing boundary layers and shown to reduce the perturbation energy of both modal and non-modal disturbances (Chevalier et al., 2007a).

### 1.2. Bypass transition

Laminar–turbulent transition in a zero-pressure-gradient boundary layer subject to high levels of free-stream turbulence is considered. Such a scenario is usually referred to as bypass since the transition occurs bypassing the exponential growth of the Tollmien–Schlichting waves. It has indeed been shown both experimentally and theoretically that the asymptotic solutions given by the classical stability analysis are not always adequate to predict transition in wall-bounded shear flows. In some cases, significant energy growth can be observed even when the flow is stable (Schmid and Henningson, 2001). This can be explained by the non-normality of the linearised operator describing the flow dynamics and the associated non-orthogonal set of eigenmodes (Reddy and Henningson, 1993). If the state of the system has a strong projection on some of these highly non-orthogonal eigenmodes the energy of the flow can experience a significant transient growth. In the case of boundary layers, the upstream perturbations which undergo the largest possible growth consist of streamwise counter-rotating vortex pairs, see Andersson et al., 1999. These vortices lift low-momentum fluid from the wall and push high-momentum fluid from the outer parts towards the plate, thus creating elongated regions of alternating accelerated and decelerated fluid, called streaks. This process of vortex tilting is also known as lift-up effect (Landahl, 1980).

After the primary energy growth due to the lift-up effect, the flow is in a more complicated laminar state where strong nonlinear interactions can come into play, leading to transition to turbulence. As the streaks grow in strength, they become susceptible to high-frequency secondary instabilities due to the presence of both wall-normal and spanwise inflectional velocity profiles (Brandt and Henningson, 2002; Brandt, 2007). These secondary instabilities manifest themselves in symmetric and antisymmetric streak oscillations, which are precursors to the formation of localised regions of chaotic swirly motion, the so-called turbulent spots (Brandt et al., 2004; Mans et al., 2007). The leading edge of a spot travels at about the free-stream velocity $U_\infty$ while the trailing edge at half this speed. The spots become therefore more elongated and eventually merge: a fully-developed turbulent boundary layer is observed. A visualisation of the transition under free-stream turbulence from the simulations presented here is provided in Fig. 1. Streamwise streaks can be seen to form close to the computational inlet, followed by streaks oscillations and turbulent spots. The flow is turbulent in the second half of the domain.

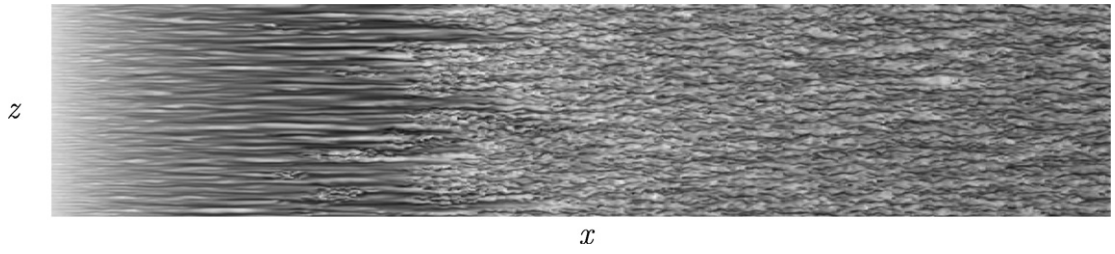


**Fig. 1.** Visualisation of the streamwise disturbance velocity component (dark colour is low velocity, light high velocity) in a plane close to the wall showing the flow development under the influence of free-stream turbulence. Streamwise extent $Re_x = [32,000,\ 570,000]$, true aspect ratio. The streamwise extent corresponds to almost the full length of a typical turbine blade.

The bypass transition scenario is observed when the boundary layer is subject to free-stream turbulence levels higher than 0.5–1% (Matsubara and Alfredsson, 2001). As described above, the flow reproduces, though on a larger scale, the near-wall dynamics of wall-bounded turbulence, see e.g. Robinson, 1991, and it is therefore an ideal test configuration in view of possible control of turbulent flows. This work represents therefore a natural extensions of the flow control studies mentioned above (Hoepffner et al., 2005; Chevalier et al., 2007a) to flows characterised by strong nonlinear interactions. An experimental demonstration of reactive control of the same scenario was recently presented by Lundell (2007). In this study, an *ad hoc* threshold-and-delay control algorithm is evaluated and shown to inhibit the growth of the streamwise velocity fluctuations for a distance downstream of the actuator position.

The paper is organised as follows. In Section 2, the control approach is presented while the numerical method, the large-eddy simulation and the free-stream turbulence generation are introduced in Section 3. The results are presented in Section 4. First, the focus will be on the validation of the LES while in the second part of Section 4 linear feedback control applied to bypass transition is considered. The paper ends with a summary of the main conclusions.

## 2. Feedback control

Linear analysis is commonly used to understand the energy growth mechanisms of perturbations in shear flows (Schmid and Henningson, 2001). However, it can also be used as a tool to design controllers that actively reduce the perturbation level and prevent or delay transition. The procedure adopted here is linear feedback control based on noisy measurements within the Linear Quadratic Gaussian (LQG) framework where a Linear Quadratic Regulator (LQR) is combined with a Kalman filter (Friedland, 1986).

Within this framework a set of linear equations is used as a model for the physical process to be controlled along with a quadratic objective function. The system is assumed to be subject to Gaussian random excitations which represent unmodelled dynamics, e.g. nonlinearities. The control requires knowledge of the full state of the system. Therefore, a state estimator, also called Kalman filter, is used to reconstruct the flow field from noisy measurements taken at the wall. To model uncertainties in the measurements, noise is assumed to contaminate the output signals. The control and estimation problem can be considered and solved separately and when combined it can be proven that this is the optimal solution (Skogestad and Postlethwaite, 2005). This is known as the separation principle. Control can be applied both in the real and in the estimated flow. The combination of an estimator and a full information controller is called compensator.

The design of a controller aims at finding the optimal mapping between the various inputs and outputs of the system in such a way that a certain objective is obtained. In this case, the system is the boundary layer flow, inputs are the external disturbances from the free stream (unknown) and the blowing/suction at the wall (known) while output is the wall measurements (known). The objective here is to reduce the kinetic energy of the perturbations in the flow.

### 2.1. Control

In this section, the design process of the full information controller is presented. Therefore, it is assumed that the exact state of the system is known.

To model the flow, the linearised Navier–Stokes equations are employed:

$$\frac{\partial \mathbf{u}}{\partial t} + \mathbf{U}\nabla\mathbf{u} + \mathbf{u}\nabla\mathbf{U} = -\nabla\pi + Re^{-1}\nabla^2\mathbf{u}, \tag{1a}$$

$$\nabla\mathbf{u} = 0, \tag{1b}$$

where $\mathbf{u} = [u \quad v \quad w]^{\mathrm{T}}$. The streamwise, wall-normal and spanwise directions are denoted $x$, $y$ and $z$, respectively, with the corresponding velocity components $u$, $v$ and $w$ and wavenumbers $k_x$, $k_y$ and $k_z$.

In Eqs. (1a), we consider small perturbations around the base flow $\mathbf{U} = [U \quad V \quad W]^{\mathrm{T}}$. To reduce the order of the system a parallel base flow is assumed $\mathbf{U} = [U(y) \quad 0 \quad 0]^{\mathrm{T}}$ and under this assumption Fourier transform can be applied along the wall-parallel directions. Thus, we can treat each wavenumber pair individually and instead of solving one problem with a large number of degrees of freedom, we solve many smaller systems. For the channel flow this assumption is exact, whereas for boundary layers, it is a good approximation due to their slow viscous growth.

To eliminate the pressure, the wall-normal velocity $v$ and the wall-normal vorticity $\eta$ formulation is adopted where the state is $(v\,\eta)^{\mathrm{T}}$. The equations that describe the dynamics are the Orr–Sommerfeld/Squire (OSS) system (see Schmid and Henningson, 2001),

$$\frac{\partial}{\partial t}\begin{pmatrix} v \\ \eta \end{pmatrix} = \begin{pmatrix} \mathscr{L}_{\mathrm{OS}} & 0 \\ \mathscr{L}_{\mathrm{C}} & \mathscr{L}_{\mathrm{SQ}} \end{pmatrix}\begin{pmatrix} v \\ \eta \end{pmatrix}, \tag{2}$$

where

$$\begin{aligned} \mathscr{L}_{\mathrm{OS}} &= [\Delta]^{-1}\left[-\mathrm{i}k_x U\Delta + \mathrm{i}k_x D^2 U + \frac{1}{Re}\Delta^2\right], \\ \mathscr{L}_{\mathrm{C}} &= -\mathrm{i}k_z DU, \\ \mathscr{L}_{\mathrm{SQ}} &= -\mathrm{i}k_x U + \frac{1}{Re}\Delta, \end{aligned} \tag{3}$$

where $U$ is the mean-flow profile, the similarity Blasius solution, $\Delta$ is the Laplacian operator $\Delta = D^2 - k^2$ with $k^2 = k_x^2 + k_z^2$ and $D$ is the wall-normal derivative. The Reynolds number $Re$ is defined by using the free-stream velocity $U_\infty$ and the local boundary-layer displacement thickness $\delta^*$,

$$Re = \frac{U_\infty \delta^*}{\nu}.$$

The control is applied through non-homogeneous boundary conditions as a model for localised blowing and suction at the wall. To adopt the same formulation as in classical control theory, the control signal is expressed in the equations as a volume forcing by a lifting procedure (Högberg and Henningson, 2002). To account for non-modelled dynamics, such as non-parallel effects and nonlinearities, external excitation is added such that two extra forcing terms appear in the equations

$$\frac{\partial \mathsf{q}}{\partial t} = \mathscr{A}\mathsf{q} + \mathscr{B}_1\mathsf{w}_1 + \mathscr{B}_2\psi, \tag{4}$$

where $\mathsf{q} = [v \quad \eta \quad \chi]^{\mathrm{T}}$, $\mathscr{B}_1\mathsf{w}_1$ is the forcing due to external excitations $\mathsf{w}_1$ of stochastic nature and $\mathscr{B}_2\psi$ is the forcing from the control signal $\psi$ and $\chi$ is the velocity at the wall. We thus have $\partial\chi/\partial t = \psi$. The operator $\mathscr{A}$ governs the dynamics of the augmented system (Chevalier et al., 2007a). Note that the control signal is the time derivative of the blowing and suction at the wall. In the case of full state-feedback control, the signal is calculated directly from the state $\mathsf{q}$ so $\mathscr{B}_2\psi = \mathscr{B}_2\mathscr{K}\mathsf{q}$ where $\mathscr{K}$ is the control gain.

The aim is to calculate the control gain $\mathscr{K}$ so that the kinetic energy of the mean-flow disturbances is minimised while at the same time the control effort is kept at low levels. To this end the following objective function is defined:

$$\mathscr{F} = \int_0^T (\mathsf{q}^*\mathscr{Q}\mathsf{q} + \psi^*\mathscr{R}\psi)\,\mathrm{d}t, \tag{5}$$

where $(\cdot)^*$ denotes the complex conjugate. The term $\mathsf{q}^*\mathscr{Q}\mathsf{q}$ corresponds to the kinetic energy of the perturbations for the specific

wavenumber pair under consideration where $\mathscr{Q}$ is the energy norm operator. The second term in Eq. (5) represents the control effort, $\mathscr{R} = l^2$, where $l$ is the actuation penalty.

As a next step, we discretise the problem so that it can be solved numerically. The control problem is now redefined as a set of one-dimensional partial differential equations, one for each wavenumber pair. Along the wall-normal direction $y$, Chebyshev polynomials are used. In the case of unbounded domains, the corresponding wall-parallel wavenumbers are a continuous set but in a bounded domain this set becomes discrete and the corresponding Fourier representation transforms from integrals into series. The series will be truncated to a wavenumber that corresponds to the resolution of the numerical simulation.

If $q$ is the discrete state vector the energy norm operator $Q$ is defined in such a way that the quantity $q^{\mathrm{H}}Qq$ approaches the kinetic energy of the system as the resolution increases. $q^{\mathrm{H}}$ is the Hermitian transpose of $q$.

The discretised system has a similar form as the continuous one

$$\frac{\partial q}{\partial t} = Aq + B_1 w_1 + B_2 \phi, \tag{6}$$

where the quantities $q$, $A$, $B_1$, $w_1$, $B_2$ and $\phi$ are the equivalent discrete counterparts of $\mathrm{q}$, $\mathscr{A}$, $\mathscr{B}_1$, $\mathrm{w}_1$, $\mathscr{B}_2$ and $\psi$.

We use the Lagrange multipliers to find the optimal solution to our problem. We define the Lagrangian

$$\mathscr{L} = \int_0^T \left[\frac{1}{2}(q^{\mathrm{H}}Qq + \phi^{\mathrm{H}}R\phi) - p\left(\frac{\partial q}{\partial t} - Aq - B_2\phi\right)\right] \mathrm{d}t, \tag{7}$$

where $p$ is the Lagrange multiplier and $R$ is the discrete versions of $\mathscr{R}$. Here, we have dropped the stochastic term $B_1 w_1$ since we will use the deterministic approach in deriving the full information control. The variation of the Lagrangian functional can be written as

$$\delta\mathscr{L} = \left(\frac{\partial \mathscr{L}}{\partial q}\right)\delta q + \left(\frac{\partial \mathscr{L}}{\partial p}\right)\delta p + \left(\frac{\partial \mathscr{L}}{\partial \phi}\right)\delta\phi. \tag{8}$$

Combining Eqs. (7) and (8) and assuming $\delta\mathscr{L} = 0$ leads to the set of equations

$$\frac{\partial \mathscr{L}}{\partial q} = \frac{\partial p}{\partial t} + A^{\mathrm{H}}p + Qq = 0, \tag{9a}$$

$$\frac{\partial \mathscr{L}}{\partial p} = -\frac{\partial q}{\partial t} + Aq + B_2\phi = 0, \tag{9b}$$

$$\frac{\partial \mathscr{L}}{\partial \phi} = R\phi + B_2^{\mathrm{H}}p = 0. \tag{9c}$$

A linear time dependent relation is assumed between the forward solution $q$ and the Lagrange multiplier $p = Xq$. Inserting this assumption into Eq. (9a) and adding Eqs. (9a) and (9c) we arrive at the differential Riccati equation,

$$\frac{\partial X}{\partial t} + A^{\mathrm{H}}X + XA - XB_2R^{-1}B_2^{\mathrm{H}}X + Q = 0. \tag{10}$$

The optimal $K$ is then given through the non-negative Hermitian solution $X$ of Eq. (10). A full derivation of the above equation is given by Lewis and Syrmos (1995). A simplified version arises if an infinite time horizon is assumed, yielding the steady-state Riccati equation,

$$A^{\mathrm{H}}X + XA - XB_2R^{-1}B_2^{\mathrm{H}}X + Q = 0 \tag{11}$$

with the control gain computed from

$$K = -R^{-1}B^{\mathrm{H}}QX. \tag{12}$$

The Riccati equation is solved for each streamwise and spanwise wavenumber pair $(k_x, k_z)$ separately and an inverse Fourier transform can be applied to visualise the control gains in physical space. It is shown by Högberg and Henningson (2002) that the control gains, relating the velocity perturbations to the control signal, are spatially localised: The control is thus dependent only on the perturbations in a limited region located upstream of the actuator.

### 2.2. Estimation

The duty of the estimator is to approximate the full three-dimensional velocity field from wall measurements in real time. Measurements are taken from the wall and the sensors responsible for the measurements include noise. The estimator can be seen as a filter operator where the equations governing the flow are used for the filtering process. Input is the measurements from the real flow and output the estimated flow. This is often called Kalman filter.

In the estimation problem, two flow fields are considered: The 'real' flow and the estimated flow (see Fig. 2). All the quantities that correspond to the estimated flow are marked with a hat $(\hat{\cdot})$.

The estimated field is assumed to fulfill the following equation:

$$\frac{\partial \hat{q}}{\partial t} = A\hat{q} - L(r - \hat{r}) + B_2\phi, \tag{13}$$

where $L$ is the measurement gain and $r$ indicates the measurements. The latter are extracted through the measurement operator $C$ and since the measurements process introduces noise, we write $r = Cq + g$ and $\hat{r} = C\hat{q}$, where $g$ is the measurement noise. The governing equation for the estimation error can be written as

$$\frac{\partial \tilde{q}}{\partial t} = (A + LC)\tilde{q} + B_1 w_1 + Lg = A_e\tilde{q} + B_1 w_1 + Lg. \tag{14}$$

The aim of the estimation problem is to minimise the difference between the real and the estimated flow, namely the estimation error $\tilde{q} = q - \hat{q}$. From the equations above, the mathematical similarity between the feedback control and the estimation problem is evident. We are looking for the optimal $L$ for which the objective function $\mathscr{F} = \tilde{r}^{\mathrm{H}}\tilde{r}$ is minimised. However, in this case we have to use the stochastic approach instead of the deterministic, since the equation is forced by stochastic inputs.

We assume that the external disturbances $w_1$ and $g$ are zero-mean stationary white noise Gaussian processes (Chevalier et al., 2007a). Since the system is forced by these stochastic processes, expected values of the relevant flow quantities are examined. In particular, for the estimation problem the covariance of the estimation error $P$ is considered and, as for the full information control, a steady state is assumed. The covariance of the error satisfies the algebraic Lyapunov equation,

$$A_eP + PA_e^{\mathrm{H}} + B_1WB_1^{\mathrm{H}} + LGL^{\mathrm{H}} = 0, \tag{15}$$

where $W$ and $G$ are the covariances of $w_1$ and $g$, respectively. This along with the objective function $\mathscr{F}$ form a new Lagrangian $\mathscr{M}$, where the traces of the covariance matrices are involved. The trace of covariance matrices correspond to rms (root-mean-square) values of the quantity under consideration (Hoepffner et al., 2005),

$$\mathscr{M} = \mathrm{trace}(PQ) + \mathrm{trace}[\Lambda(A_eP + PA_e^{\mathrm{H}} + LGL^{\mathrm{H}} + B_1WB_1^{\mathrm{H}})], \tag{16}$$

where $\Lambda$ is the Lagrange multiplier. The first term in Eq. (16) is the objective function to be minimised and the second is the constraint coming from the Lyapunov equation satisfied by the covariance error. At the stationary point of $\mathscr{M}$

$$\frac{\partial \mathscr{M}}{\partial P} = Q + (A + LC)^{\mathrm{H}}\Lambda + \Lambda^{\mathrm{H}}(A + LC) = 0, \tag{17a}$$

$$\frac{\partial \mathscr{M}}{\partial \Lambda} = (A + LC)P + P(A + LC)^{\mathrm{H}} + B_1WB_1^{\mathrm{H}} + LGL^{\mathrm{H}} = 0, \tag{17b}$$

$$\frac{\partial \mathscr{M}}{\partial L} = 2\Lambda(PC^{\mathrm{H}} + LG) = 0. \tag{17c}$$

The solution to this optimisation problem is given by the numerical solution $P$ of a Riccati equation similar to that arising in the feedback control problem,

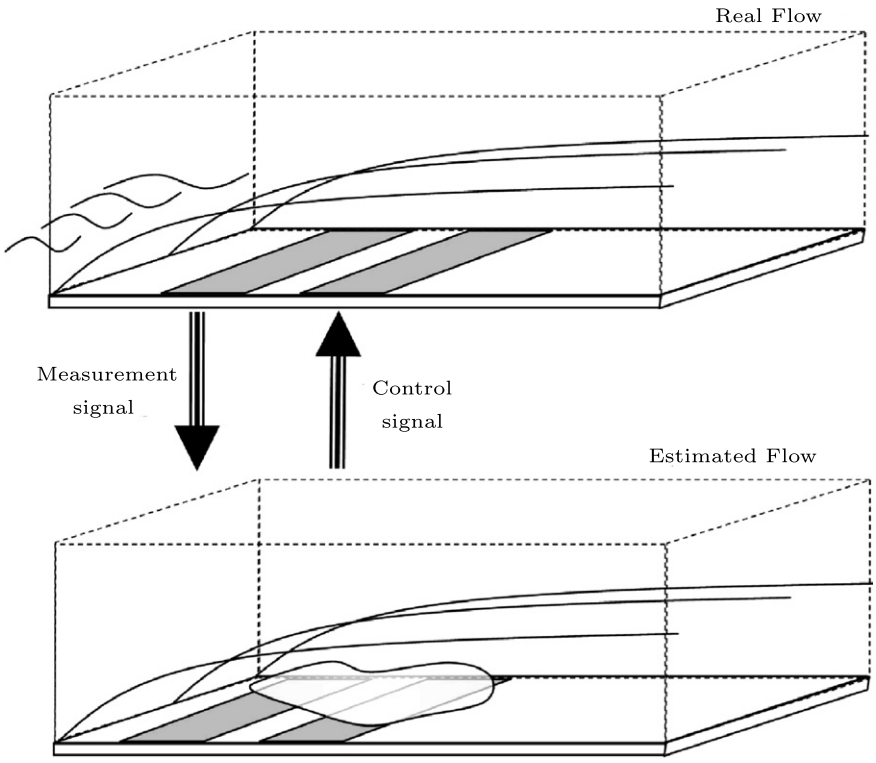


**Fig. 2.** A schematic drawing of the compensator. Wall measurements are taken in the real flow and compared to those from the estimator. The control signal is computed based on the reconstructed velocity field and applied in the real flow.

$$AP + PA^{H} - PC^{H}G^{-1}CP + B_1WB_1^{H} = 0 \tag{18}$$

with the estimation feedback gain given by $L = -PC^{H}G^{-1}$. For a similar derivation, see also Bagheri et al., in press.

In the computations presented, three quantities are measured at the wall, namely the streamwise and spanwise skin friction and the pressure:

$$\tau_x = \tau_{xy}|_{\text{wall}} = \frac{1}{Re}\frac{\partial u}{\partial y}\bigg|_{\text{wall}}, \tag{19a}$$

$$\tau_z = \tau_{zy}|_{\text{wall}} = \frac{1}{Re}\frac{\partial w}{\partial y}\bigg|_{\text{wall}}, \tag{19b}$$

$$p_{\text{wall}} = \Delta_{xz}^{-1}\left(\frac{1}{Re}\frac{\partial^3 v}{\partial y^3}\right)\bigg|_{\text{wall}}, \tag{19c}$$

where $\Delta_{xz}^{-1}$ denotes the formal inverse of the wall-parallel Laplacian.

The Kalman filter presented here is the optimal estimation in a linear setting. To apply the above theory in a highly nonlinear case, one may use the full (nonlinear) equations when solving the estimation problem (13) while the gains used are computed with the linear theory. This is the extended Kalman filter and it is expected to be more accurate than the standard Kalman filter.

### 2.3. Compensator

The compensator is the combination of full information control and state estimation. The measurements taken from the real flow are communicated to the estimator where they are used to compute the forcing needed to reproduce the perturbations present in the real flow. The actuation signal is computed from the estimated flow and it is applied to both the estimated and the real flow. Although computed for linear systems, the control and estimation are applied to the full nonlinear Navier–Stokes equations (Högberg et al., 2003c).

The compensator problem as it was stated here accounts only for parallel flows as there is no explicit streamwise dependence in the OSS operator. Further, it assumes that measurements are taken and actuation is applied continuously over the whole domain. This theory is applied to a spatial boundary layer and both measurements and actuation are available only on a part of the domain (see Fig. 2). Two regions need to be specified, one for the control and one for the estimator. For both regions, the local laminar velocity profile is used as a base flow in the OSS operator. The flow is assumed to be locally parallel around these locations in order to solve the control and estimation problems. Once the control and estimation gains are calculated, the actuation forcing is limited to the actuation region by a smooth transfer function in physical space with two smooth step functions around the chosen locations (Chevalier et al., 2007a).

## 3. Simulation approach

### 3.1. Numerical method

For the present computations, the three-dimensional, time dependent, incompressible Navier–Stokes equations are solved using a spectral method (Chevalier et al., 2007b). The algorithm uses Fourier representation in the streamwise and spanwise directions and Chebyshev polynomials in the wall-normal direction, together with a pseudo-spectral treatment of the nonlinear terms. Dealiasing using the 3/2-rule is employed in the wall-parallel (Fourier) directions, whereas a slightly increased resolution is used in the wall-normal direction to reduce aliasing errors. The time is advanced with a four-step low-storage third-order Runge–Kutta method for the nonlinear terms and all the forcing contributions, and a second-order Crank–Nicolson scheme for the linear terms and boundary conditions. To correctly account for the downstream boundary-layer growth the spatial simulation approach is necessary. This requirement is combined with the periodic streamwise boundary condition by the implementation of a *fringe* region (Nordström et al., 1999; Lundbladh et al., 1999). In this region,

positioned at the downstream end of the computational box occupying approximately 10% of the flow domain, a volume forcing is smoothly raised from zero to force the flow from the outflow to the desired inflow condition. The inflow consists of the laminar Blasius boundary layer with superimposed spatially and temporally varying disturbances, i.e. the free-stream turbulence in the present case.

#### 3.1.1. MPI implementation and performance

The numerical code described above is parallelised to run on distributed-memory architectures (i.e. clusters) using the Message Passing Interface (MPI). As detailed in Section 2.3, the simulation of the estimator and compensator actually requires the time-advancement of two flow fields, i.e. the "real" flow field and the estimated field. These two fields are coupled by the measurements and the control actuation (in case of compensator), and feature different inflow conditions and may have different spatial resolution and domain size. In the present implementation this is achieved by having two simulations running simultaneously on a subset of the available processors; the two simulations have two different executables, compiled with different options but running within the same MPI environment. Information exchange is then accomplished using distinct messages sent between the two codes. Details on the implementation can be found in Seyed (2007).

To give an estimate of the computational cost, the details of a typical simulation are now outlined. The "real" flow is simulated via direct numerical simulation (DNS) discretised on a domain with approximately $20 \times 10^6$ grid points. The corresponding estimator simulation can be run as a large-eddy simulation (LES) (see Section 3.2 below) with a lower resolution of approximately $2.5 \times 10^6$ grid points. In this example, the DNS is run on 24 processors, and the estimator LES on 6 processors, i.e. employing a total of 30 processors. The necessary runtime in order to obtain fully converged statistics (simulated time $\Delta t = 4000$) is about 300 h on 30 processors corresponding to 9000 CPU hours.

### 3.2. Subgrid scale modelling

The fine grids (and the corresponding small time steps) necessary in the DNS of turbulent flows at moderate to high Reynolds numbers give rise to very high computational costs. Therefore, other approaches based on large-eddy simulations (LES) have been developed to be able to simulate transitional and turbulent flows in large-enough domains and at high *Re*. In LES the mesh size is chosen considerably larger than for DNS. This implies that the structures present in the flow are only resolved above a certain size corresponding to the cutoff wavenumber $\omega_{c,\mathrm{grid}}$. This length scale is chosen to be small enough to capture well the structures that are involved in the physical phenomena under investigation. On the other hand, the scales below the cutoff scale are not resolved on the numerical grid, but their influence due to nonlinearity onto the resolved scales must be modelled by a subgrid-scale (SGS) model. For flows with solid walls, the thin boundary layers adjacent to the walls need to be resolved in both DNS and LES for accurate results. Therefore, even LES requires a substantial computational effort, albeit lower than DNS: A typical resolution for an LES is approximately 1–20% of a corresponding fully-resolved DNS.

Formally, the solution in an LES calculation is obtained by applying a generic low-pass filter $G^P$ with a certain filter width $\Delta$ suitable for the problem under consideration,

$$\bar{u}_i(x) := G^{\mathrm{P}} * u_i := \int_{\mathscr{V}} G^{\mathrm{P}}(x, x', \Delta) u_i(x') \mathrm{d}x', \tag{20}$$

where $\bar{u}_i(x)$ denotes the filtered quantity and $\mathscr{V}$ the computational domain. $G^{\mathrm{P}}$ is referred to as the primary LES filter. The governing momentum equations for the filtered quantities become

$$\frac{\partial \bar{u}_i}{\partial t} + \frac{\partial \bar{u}_i \bar{u}_j}{\partial x_j} = -\frac{\partial \bar{p}}{\partial x_i} - \frac{\partial \tau_{ij}}{\partial x_j} + \frac{1}{Re} \frac{\partial^2 \bar{u}_i}{\partial x_j \partial x_j} \tag{21}$$

together with filtered incompressibility constraint

$$\frac{\partial \bar{u}_i}{\partial x_i} = 0. \tag{22}$$

The interaction between the resolved and unresolved scales is given by the SGS stresses,

$$\tau_{ij} = \overline{u_i u_j} - \bar{u}_i \bar{u}_j, \tag{23}$$

which is an unclosed term and thus has to be modelled based on the filtered velocity field $\bar{u}_i$. In most LES approaches the primary filter is not applied explicitly, but rather given by the implicit filter due to the lower grid resolution.

The ADM-RT model used here acts on the velocity components directly. The model employs the relaxation term proposed in the context of the approximate deconvolution model (ADM) (Stolz and Adams, 1999). It has been shown in, e.g. Schlatter et al. (2006a) and Schlatter et al. (2006b) that for spectral simulations the deconvolution operation applied in the ADM approach is not necessary. Therefore, the SGS force due to the ADM-RT model is given by (Schlatter et al., 2004)

$$\frac{\partial \tau_{ij}}{\partial x_j} = \chi H_N * \bar{u}_i \tag{24}$$

with $\chi$ being the model coefficient. $H_N$ denotes a high-order three-dimensional high-pass filter (Stolz et al., 2001), and the symbol $*$ stands for convolution in physical space, i.e. a multiplication with the respective transfer function $\widehat{H}_N$ in Fourier space.

The high-pass filter $H_N$ used in the present work is obtained by the repeated application of a low-pass filter $G$ according to

$$H_N = (I - G)^{N+1}, \quad N > 0. \tag{25}$$

Typically, $G$ is chosen as the low-order low-pass filter suggested by Stolz et al. (2001). The cutoff frequency is defined as $\widehat{G}(\omega_c) = 1/2$ and can be adjusted. For the present results, $\omega_c = 2\pi/3$ and $N = 5$. $H_N$ is at least of order $r(N+1)$ with $r$ being the order of $G$. The latter is at least $r = 3$ on non-equidistant grids.

$\chi$ is the model coefficient which is set to a constant value herein motivated by previous studies showing little dependency of the results on the actual value of the coefficient (see e.g. Schlatter et al., 2006b). If the model coefficient $\chi$ is chosen inversely proportional to the time-step size the relaxation term has a similar effect as a filtering of the velocities after every time step, as mentioned in Stolz and Adams, 1999.

The relaxation term $\chi H_N^* \bar{u}_i$ is proportional to the small-scale velocity fluctuations in the flow field. Therefore, it will damp out these oscillations leading to a drain of kinetic energy from the smallest resolved scales.

The ADM-RT model proved to be accurate and robust in predicting transitional and turbulent incompressible flows with spectral methods (Schlatter et al., 2004; Schlatter et al., 2006b). Note that the relaxation-term model is related to the spectral vanishing viscosity approach (Karamanos and Karniadakis, 2000). Due to the high-order filter $H_N$ with a cutoff frequency of $\omega_c \approx 0.86\pi$ only the smallest represented eddies are affected, whereas the larger, energy-carrying scales are not directly influenced by the model contributions.

### 3.3. Free-stream turbulence generation

The boundary layer considered here is subject to external disturbances, in particular free-stream turbulence. To generate this inflow a superposition of eigenmodes from the continuous spectrum of the OSS operator is used (Jacobs and Durbin, 2001; Brandt

et al., 2004). In the present implementation disturbances can be introduced in the flow in three different ways: forcing them in the fringe region, with a body force as in the estimation problem, or via blowing and suction at the wall by a non-homogeneous boundary condition as done in the control problem. The free-stream turbulence is forced at the inflow by adding the modes to the laminar base-flow profile in the fringe region.

Detailed description of the procedure adopted can be found in Brandt et al. (2004). Here, the free-stream generation is shortly outlined. A three-dimensional wave vector $\mathbf{k} = (k_x, k_y, k_z)$ is associated to each eigenfunction of the continuous spectrum where, $k_x$ and $k_z$ are defined by the normal-mode expansion along the wall-parallel directions of the underlying linear problem while the wall-normal wavelength is determined by the eigenvalue along the continuous spectrum. If Taylor's hypothesis is applied the streamwise wavenumber $k_x$ can be replaced by a frequency $\omega = k_x U_\infty$ and the disturbance signal is written as

$$u_{\text{dist}} = \sum A_N \hat{u}_N(y) \mathrm{e}^{\mathrm{i}k_z z + \mathrm{i}k_x x - \mathrm{i}\omega t}, \tag{26}$$

where the wall-normal wavenumber $k_y$ is implicit in the shape of the eigenfunction $\hat{u}_N(y)$ (Grosch and Salwen, 1978). The complex wavenumber $k_x$ is determined by the dispersion relation once the real wall-normal wavenumber $k_y$ and the real wavenumbers $k_z$ and $\omega$ are selected according to the procedure described below. The wavenumbers pertaining to the modes used in the expansion are selected by defining a number of spherical shells of radius $|k|$ in the wavenumber space $(\omega, k_y, k_z)$. Forty points are then placed at equal intervals on the surface of these spheres. The coordinates of these points define the wavenumbers of the modes used in the expansion above. The complex coefficients $A_N$ provides random phase but a given amplitude. The amplitude $|A_N|$ is in fact the same for all modes on each shell and is chosen to reproduce the Von Kármán spectrum,

$$E(k) = \frac{2}{3} \frac{a(kL_l)^4}{(b + (kL)^2)^{17/6}} L_l Tu. \tag{27}$$

This spectrum is for large scales asymptotically proportional to $k^4$, whereas it matches the Kolmogorov-(5/3)-law for small scales. In the expression above, $Tu$ is the turbulence intensity, $L_l$ is a characteristic integral length scale such that $k_{\max} = 1.8/L_l$ where $k_{\max}$ is the wavenumber of maximum energy and $a$, $b$ two normalisation constants.

#### 3.3.1. Free-stream turbulence generation in the LES

Due to the lower resolution employed for the LES runs, the imposed turbulence spectrum at the inlet has to be adapted. To obtain results that are as close to the DNS as possible, it was decided to use exactly the same set of modes and the same random phases on all the various grids, without any modification of the turbulence intensity level at the inlet. Modes with wavenumbers too large to be resolved on a given coarser LES grid were discarded and consequently not forced at the inlet. All the other parameters specifying the inlet spectrum, i.e. length scale, choice of modes and the individual scaling of the modes, are the same on all grids. This leads to the observation that the measured turbulence intensity at the inlet is smaller for coarser grids, because less modes are actually forced. To obtain the true $Tu$ one had to also include the unresolved fluctuations, which are however not available during an LES. The results show that the transition process is not crucially influenced by that difference in inlet $Tu$. If, on the other hand, the resolved $Tu$ at the inlet is adapted to exactly match the level on the finest (i.e. DNS) grid, premature transition corresponding to the higher turbulence levels is observed. The explanation for this behaviour is that the receptivity of the boundary layer is mainly dominated by low-frequency modes of the free stream. The amplitudes of these modes, which are resolved on both the DNS and LES grids, should therefore not be modified.

**Table 1**
Different computational boxes used

| Box | Method | $L_x \times L_y \times L_z$ $\delta_0^*$ | $N_x \times N_y \times N_z$ (resolution) |
|---|---|---|---|
| Small | DNS | $1000 \times 60 \times 50$ | $1024 \times 121 \times 72$ |
| Small | LES | $1000 \times 60 \times 50$ | $256 \times 121 \times 36$ |
| Medium | LES | $2000 \times 60 \times 90$ | $512 \times 121 \times 64$ |
| Large | LES | $2000 \times 60 \times 180$ | $512 \times 121 \times 128$ |
| X-large | LES | $4000 \times 60 \times 180$ | $1024 \times 121 \times 128$ |

Resolution for each box dimensions and type of simulation.
The box dimensions include the fringe region and are non-dimensionalised with respect to the displacement thickness $\delta_0^*$ at the inflow ($Re_{\delta_0^*} = 300$).

### 3.4. Simulation parameters

The parameters defining the problem are the Reynolds number, the intensity and the integral length scale of the free-stream turbulence and the size of the computational box. The inflow Reynolds number $Re_{\delta_0^*}$, defined using the displacement thickness of the boundary layer at the inflow of the computational domain, was chosen to be 300 for all cases under consideration.

The different computational boxes used are reported in Table 1. Direct numerical simulations were only performed in the small box, while the largest boxes were used to allow the transition to turbulence to occur within the computational domain. The latter computational domains are thus used for the parametric study of bypass transition and its control. The medium-size box was used when investigating the influence of limiting the control signal (see Section 4.2.1).

The code was run in four different modes, corresponding to four different physical problems: no control (used as reference case), full information control, estimation without control and compensator, i.e. control based on estimation.

## 4. Results

Based on the theory and numerical methods presented in the previous sections, simulations of transition in a flat-plate boundary layer subject to free-stream turbulence are performed. Linear feedback control is then applied to the flow in order to delay transition. Both LES and DNS are presented here and all the statistics presented are obtained by averaging in time and in the spanwise direction.

In the following results the streamwise coordinate is indicated by the Reynolds number based on the distance from the leading edge,

$$Re_x = \frac{U_\infty x}{\nu} = \frac{Re_{\delta^*}^2}{1.7208},$$

where the value of $\delta^*$ for the laminar Blasius solution is used. All the quantities presented are non-dimensionalised with the free-stream velocity, $U_\infty$, the viscosity, $\nu$ and the displacement thickness at the inflow of the computational domain $\delta_0^*$.

### 4.1. LES validation

In a first step, the possibility to reduce the numerical resolution and consequently replacing the effect of the non-resolved scales by a subgrid-scale model (see Section 3.2) is explored. In particular, additional to fully-resolved DNS, two different modelling approaches are considered: under-resolved DNS without model where the interaction between the resolved and unresolved scales is essentially neglected and the ADM-RT model. This SGS model

has been shown to perform particularly well with transitional wall-bounded flows (Schlatter et al., 2006b). All the LES presented in this section are performed with a free-stream turbulence intensity of $Tu = 4.7\%$ on the "Large LES" grid given in Table 1. The reference DNS data is taken from Brandt et al., 2004 using the same numerical method and inflow turbulence generation algorithm.

Fig. 3 shows the evolution of the statistically averaged skin friction coefficient $c_f$ and the shape factor $H_{12}$ as a function of the downstream distance $Re_x$. The skin friction coefficient gives a measure on how well the near-wall flow structures can be represented, whereas the shape factor, being the ratio between the boundary-layer displacement thickness and the momentum thickness, describes the flow development and structural reordering of the boundary layer during laminar–turbulent transition further away from the wall.

The evolution of the skin friction (Fig. 3a) clearly shows that the no-model approach without employing a subgrid-scale model leads to inaccurate results. This behaviour of under-resolved simulations is however well-known from other studies: The reduced dissipation present in the flow leads to an increased fluctuation level at the scales close to the numerical cutoff; in case of flows undergoing transition this increased energy may be causing premature breakdown. Usually, increased values of the wall-normal velocity gradient close to the wall lead to a dominant overshoot of the skin friction, until the flow has settled down to a new equilibrium state accounting for the missing dissipation in the small scales. The ADM-RT model with a constant model coefficient however is seen to provide an accurate prediction of the skin friction throughout the laminar initial phase dominated by the streaky structures ($Re_x < 150,000$), the stage dominated by the intermittent appearance and growth of turbulent spots ($Re_x < 300,000$), and the fully-developed turbulent region thereafter.

The shape factor given in Fig. 3b confirms the previous findings: the initial phase ($Re_x < 100,000$) characterised by only minor disturbances within the boundary layer is predicted accurately also by the no-model LES. However, as soon the boundary-layer distortion becomes too large, the under-resolved DNS will immediately break down to turbulence. It is interesting to note that the SGS model feature a slight departure from the reference level of $H_{12}$ between $Re_x = 100,000$ and $Re_x = 170,000$; however the final stages of transition seem not to be influenced.

A comparison of an instantaneous visualisation of a wall-parallel plane at $y = 2\delta_0^*$ from both DNS and ADM-RT is presented in Fig. 4. Note that for both simulations the same amplitudes and phase shifts in the inlet free-stream turbulence have been used (see Section 3.3.1), consequently the flow structures can be directly compared between DNS and LES. The most obvious feature is that the LES data looks slightly blurred, which is a natural consequence of the lower resolution. Nevertheless, many of the flow structures present in the DNS flow field can also be detected in the LES field, and vice versa: the shape and location of the dominant strong streaks, the intermittent breakdown to localised turbulent spots, and a calm region even more downstream than the first turbulent patch. This figure clearly shows that – despite the lower resolution used in the LES – a good prediction of the dominating flow physics and the processes leading to turbulent breakdown can be obtained

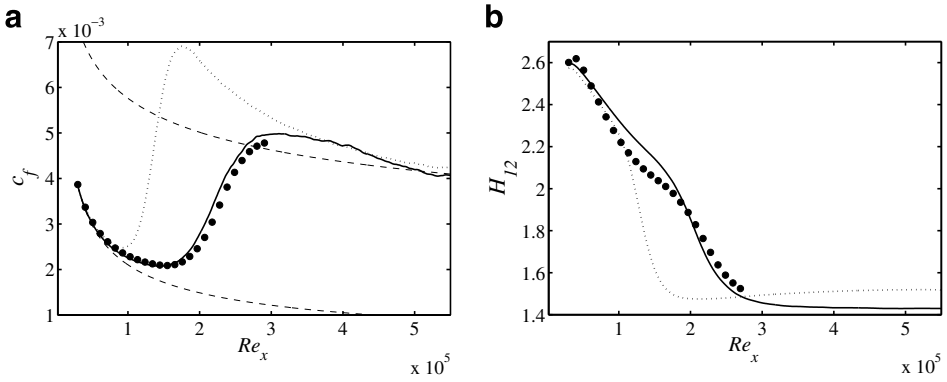


**Fig. 3.** Integral quantities during bypass transition ($Tu = 4.7\%$) for different SGS models. (a): skin-friction coefficient $c_f$, (b): shape factor $H_{12}$. ADM-RT, ; no-model LES, ·····; DNS, • (Brandt et al., 2004). The thin dashed lines correspond to analytical correlations for both laminar and turbulent boundary-layer flow.

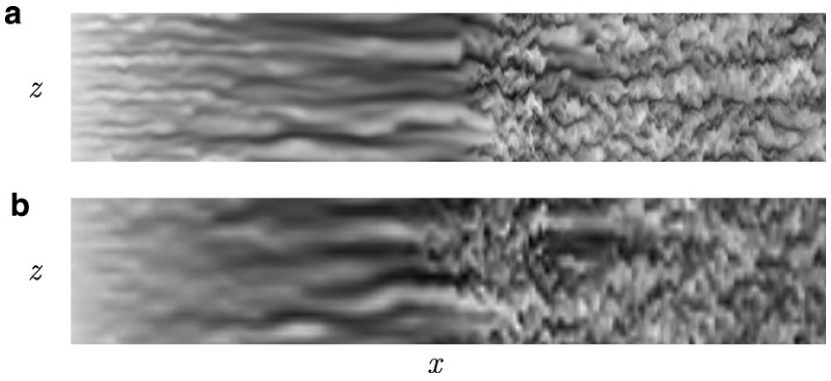


**Fig. 4.** Instantaneous streamwise velocity in a plane parallel to the wall. (a): DNS. (b): LES using ADM-RT. Light colour indicates low velocity, dark colour high velocity. Streamwise extent $Re_x = [32,000,\ 300,000]$, spanwise extent enlarged by a factor of 5.

via appropriate subgrid-scale modelling. It can also be shown that the LES is able to capture the instantaneous structures just prior to turbulent breakdown.

### 4.2. Full information control

Results on linear feedback control of a boundary layer subject to free-stream turbulence are reported next. The design parameters for the compensator problem are reported in Table 2 and will be discussed when presenting the results for each specific case.

The first step when applying control is to design a reasonably good full-information controller. This can be used as reference for the compensation, since the best possible performance is expected when the whole flow field is known. This case is also used as a benchmark for LES: Since LES is used for most of the simulations, it is considered important to evaluate the SGS model against DNS data not only in the general case without control, but also in the case of full information control. Further, in order to later compare these results to those from the compensator, the blowing and suction strip are placed further downstream, so that there will be enough space for the measurement region at the beginning of the computational domain, see Table 2. Note that in the following figures the gray areas correspond to the regions where measurements are taken, and blowing and suction is applied, respectively. The simulations in the remaining part of this section are performed with a turbulence level $Tu = 3.0\%$ except the results in Fig. 6 where $Tu = 4.7\%$.

In Fig. 5, the wall-normal maximum of the streamwise velocity perturbation is shown for both DNS and LES of the uncontrolled case as well as for the two cases with full information control. This quantity is selected since it indicates the growth of the streaks inside the boundary layer. It can be clearly seen that the control is able to inhibit the streak growth and that using LES-(ADM-RT) gives similar decrease of the streak amplitude as in the fully-resolved DNS. Slight differences between LES and DNS can be noticed at the inlet of the domain. This can be explained by noting that the wall-normal maximum of the *rms* value is a very sensitive quantity, involving both the location and the amplitude of the fluctuations. Indeed mean quantities, like the skin friction, would not show any difference at all in such a plot.

A study to investigate the influence of the length of the control region on the transition delay was also performed. The free-stream turbulence level was chosen to be 4.7% to be able to reproduce the full transition process within the small computational domain (Barri, 2006). The initial and final locations of the control region are reported in Table 3, whereas the value of the wall-normal maximum of the streamwise velocity fluctuations and the skin friction are displayed in Fig. 6 for the three cases under consideration together with the reference uncontrolled case. It can be noticed in Fig. 6a that with a longer control domain, it is possible to reduce the streak growth even more. The effect of the control is more pronounced when looking at the friction coefficient $c_f$ as shown in Fig. 6b. By comparing the two plots it can be deduced that the large values of streamwise velocity fluctuations at the end of the computational domain are not associated to a fully turbulent flow. The results farther show that for the longest control region the streak growth is indeed quenched for a larger distance but the downstream recovery is faster and the differences between the cases "Medium" and "Long" are attenuated further downstream.

In order to understand the physical mechanism behind the control, instantaneous features that appear in the controlled field are examined. In Fig. 7, the streamwise velocity component on a plane parallel to the wall at $y = 2\delta_0^*$ (Fig. 7a) along with the wall-normal velocity component at the wall (Fig. 7b) indicating the control actuation via wall blowing and suction is displayed. From these two instantaneous images of the flow one can see the correlation between the flow state and the control signal. In the case of a high-speed streak blowing is induced from the controller. This causes the flow downstream of the actuation to settle in a more stable state since the fast moving fluid is forced to move upwards away from the wall. The opposite action is happening for low-speed streaks, i.e. the controller is applying suction to move high-speed fluid from the free stream to cancel the region of decelerated flow. One other aspect to note from this figure is that most of the control effort is concentrated at the beginning of the control region in agreement with the results by Chevalier et al. (2007a).

#### 4.2.1. Limiting of control signal

When extending the linear control to these highly nonlinear scenarios, problems may arise and *ad hoc* tuning may be necessary. For our case, Brandt and Henningson (2004) observed that, if too strong localised blowing is applied, turbulent spots may be induced by local instabilities due to wall-normal inflectional profiles already inside the control region. An improvement of the transition delay can therefore be expected by limiting the blowing at the wall. This was implemented in the numerical code by imposing an artificial clipping to the control signal

$$v(x,y,z,t)|_{y=0} = \min\{v(x,y,z,t)_{y=0}, v_{\max}\}|.$$

**Table 2**
Control penalties, estimation sensor noise, measurement-strip position, actuation-strip position and location of the base flow target profiles for the estimator and the controller

| Estimation | | Control | |
|---|---|---|---|
| Sensor noise | | penalties | |
| $p$ | 50 | $l$ | $10^2$ |
| $\tau_x$ | 0.07 | $r^2$ | 0 |
| $\tau_z$ | 0.07 | | |
| $Re_{x_{start}}$ | $6.04 \times 10^4$ | $Re_{x_{start}}$ | $1.95 \times 10^5$ |
| $Re_{x_{end}}$ | $1.50 \times 10^5$ | $Re_{x_{end}}$ | $2.85 \times 10^5$ |
| Location of target profile | $1.05 \times 10^5$ | location of target profile | $2.40 \times 10^5$ |

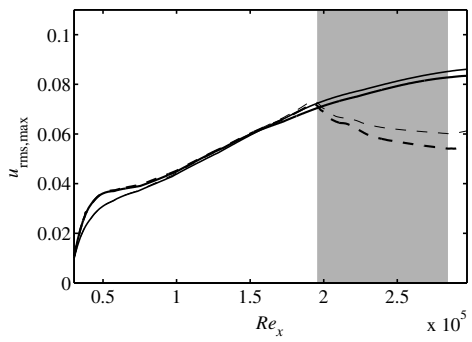


**Fig. 5.** Wall-normal maximum $u_{rms}$. no control DNS, —; no control LES, —; control DNS, – – – –; control LES, – – – –.

**Table 3**
Study on the influence of the control region length

| | Start ($Re_x$) | End ($Re_x$) |
|---|---|---|
| No control | – | – |
| Short | $5.3 \times 10^4$ | $1.4 \times 10^5$ |
| Medium | $5.3 \times 10^4$ | $1.9 \times 10^5$ |
| Long | $5.3 \times 10^4$ | $2.3 \times 10^5$ |

The initial and final location of the control region are given in units of $Re_x$.

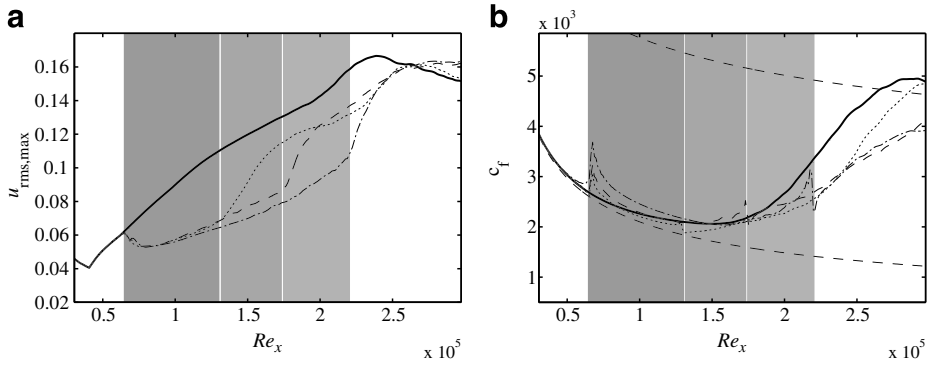


**Fig. 6.** Wall-normal maximum $u_{rms}$: (a) and skin friction coefficient $c_f$ (b). no control, ; short, ·····; medium, – – – –; long, –·–.

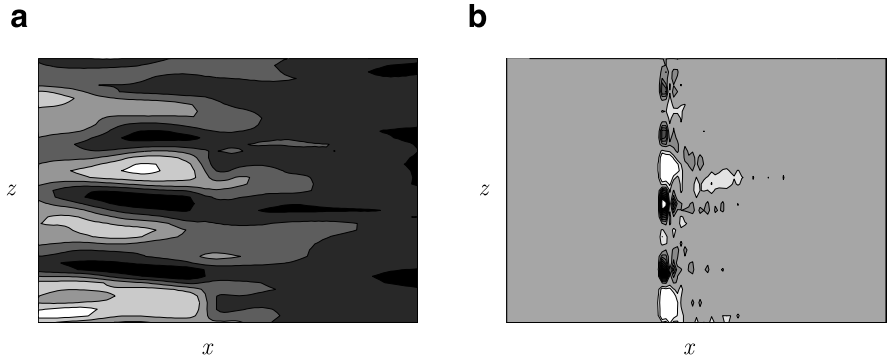


**Fig. 7.** (a): Instantaneous streamwise velocity at $y = 2\delta_0^*$. (b): corresponding control signal. The levels of the contours are $u = [0.3U_\infty, 0.6U_\infty]$ for (a) and $v = [-2 \times 10^{-2}U_\infty, 5 \times 10^{-3}U_\infty]$ for (b). White corresponds to the minimum value and black to the maximum.

The clipping threshold $v_{max}$ is set to $0.01U_\infty$, for cases where the (unlimited) maximum of the blowing at the wall occasionally reaches values of the order of $0.02U_\infty$. The value of $v_{max}$ is chosen by examining the instantaneous values of the blowing in cases where transition was triggered by the wall actuation.

The comparison between the optimal linear control and control with limited blowing is displayed in Fig. 8, where the evolution of the wall-normal maximum of the streamwise velocity fluctuations is depicted for cases with and without clipping. The performance of the control is on average improved by limiting the blowing; analysis of the instantaneous velocity fields reveals that this is due to the absence of the localised spots intermittently induced by the strong control signals and not by an overall decrease of the streak amplitudes, or increase of the actuation efficiency. The results presented in the following are all obtained by limiting the blowing at the wall.

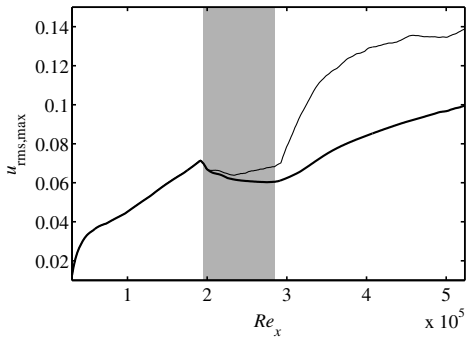


**Fig. 8.** Wall-normal maximum $u_{rms}$. Control with clipping of the blowing, —; Control without the clipping blowing, –.

### 4.3. State estimation

The construction of the estimator involved extensive tuning of several parameters associated with the theoretical tools described in Section 2.2. In particular, these parameters are: the covariance matrix as a model for the stochastic disturbances involved in the estimation process, the sensor noise quantifying the confidence in the measurements taken and the length of the estimation region.

The covariance matrix is essential for the estimator (see Eq. (18)). In the ideal case, the measurements indicated in Eq. (19c) would uniquely identify the current state of the system (Bewley and Protas, 2004). This is not the case since there are unknown initial conditions, unknown external disturbances and noise corrupting the measurements. To improve the estimation in the case of free-stream turbulence, the variance of the external disturbances needed to be extended further out in the free stream if compared to that used in Chevalier et al. (2007a). A diagonal matrix was used as covariance matrix for the external disturbances. For the covariance of the wall measurements a simple function proportional to the boundary-layer velocity profile was selected.

The parameters that define the strength of the forcing that is applied to the system are the sensor noise. The tuning of these parameters was also performed by testing different sets of values; the set of values yielding the best performance is reported in Table 2. Note that a relatively large value of the pressure sensor is needed to achieve good estimation. This limits the use of this measurement and can be explained by the fact that the pressure at the wall appears to be more sensitive to the free-stream turbulence than to the streaks inside the boundary layer.

One would expect that the longer the measurement strip the better the estimation since more information from the flow is available. However, since the gains are computed for a parallel

flow, this may not be the case and above a certain length the quality of the estimation degrades. The optimal length was found to be 500 approximately $\delta_0^*$ units. Further, it was found that at these high levels of perturbation, estimation works better if the forcing is active only on the scales that correspond to the streaks. Thus, the gains where rescaled in wavenumber space with a two-dimensional Gaussian function. The parameters of this function were determined by applying two-dimensional Fourier transforms along the wall-parallel directions to the flow fields to be estimated and extracting the wavenumbers of richest energy content. One example of this weighting function is shown in Fig. 9. The gains are focused around wavenumber $k_x = 0.0$ in the streamwise direction, which corresponds to infinitely long structures and around $k_z = 0.4$ which corresponds to the spanwise width of the most energetic structures, namely the streaks.

Two different criteria were used to determine the performance of the estimator. The first was visual inspection of the instantaneous velocity fields: One example of this comparison can be seen in Fig. 10, where the streamwise velocity in a plane parallel to the wall is displayed for the real and the estimated flow. It can be seen in the figure that the main features of the incoming streaks are well reproduced in the estimated field. A second, more systematic way, is to calculate the estimation error given by

$$\epsilon = \frac{\int_\Omega (q - \hat{q}) \mathrm{d}\Omega}{\int_\Omega (q)\, \mathrm{d}\Omega}, \tag{28}$$

where $\Omega$ is the region selected to evaluate the estimation error. In Fig. 11, the estimation error is plotted as a function of time. In this case the error is computed in a plane parallel to the wall, $y/\delta_0^* = 2$, over the whole region where the control will be applied. This is selected as the most relevant area in terms of compensator performance since the flow in this region is used to compute the control signal. It can be seen in the figure that the estimation is converging toward values of $\epsilon \approx 0.3$ after an initial transient of about 400 time units.

The wall-normal maximum of the streamwise velocity perturbation is shown for both the real and the estimated flow in Fig. 12. The perturbations are weaker in the estimated flow, a

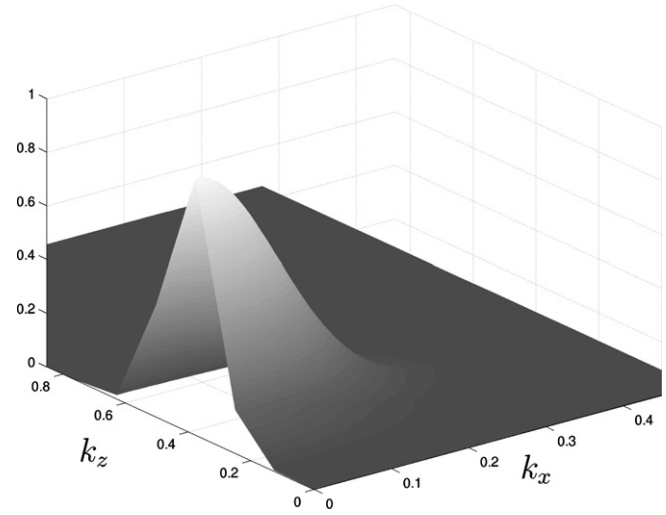


**Fig. 9.** The Gaussian function scaling the estimation gains in wavenumber space. The centre of the Gaussian is at $k_x = 0$ and $k_z = 0.4$ in units of $\delta_0^{*-1}$.

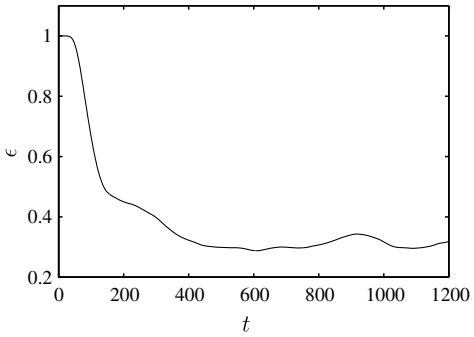


**Fig. 11.** Estimation error according to Eq. (28).

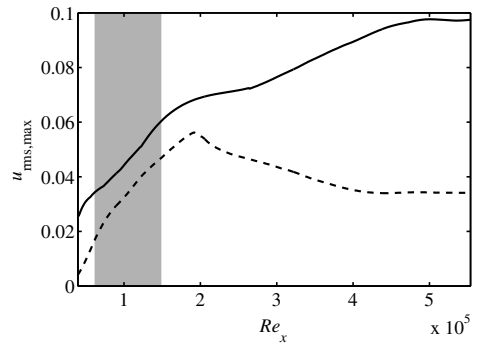


**Fig. 12.** Wall-normal maximum of $u_{\mathrm{rms}}$. Real flow, ; Estimated flow, – – – –. The shaded area indicates the measurement region.

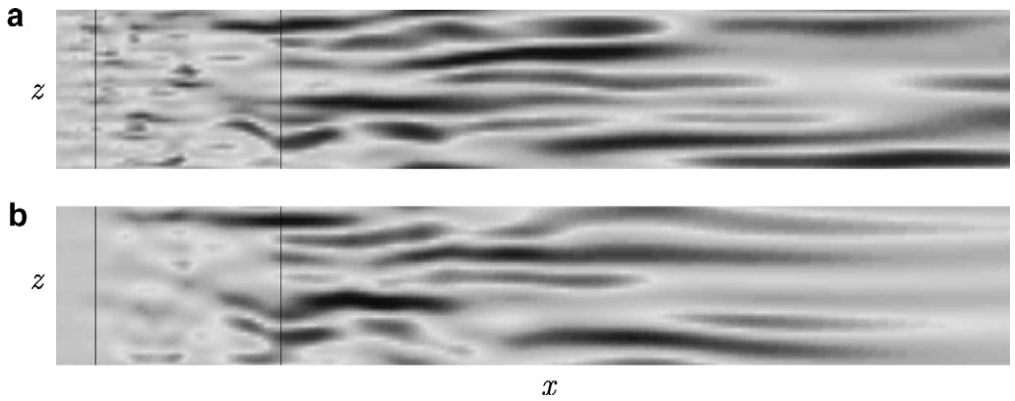


**Fig. 10.** Instantaneous streamwise velocity fields. (*a*): real flow; (*b*): estimated flow. The measurement strip is indicated with two vertical lines. Streamwise extent $Re_x = [32,000,\ 570,000]$, spanwise extent enlarged by a factor of 5.

strong estimation forcing leading directly to transition in the estimator simulation. In the real flow, the streaks are forming and growing also downstream of the estimation region, whereas in the estimated flow the streaks decay downstream of the measurement region. This can be explained by the fact that the free-stream turbulence is continuously forcing the streaks all along the plate whereas the estimation forcing is active only in a limited streamwise region, i.e. the gray area in the plot.

In Fig. 13, the wall-normal profiles of $u_{\mathrm{rms}}$ at different streamwise locations are shown. Again it can be seen that the streaks are weaker in the estimated flow than in the real flow, and that the difference between the two fields increases further downstream. Perturbations in the free stream are not reproduced in the estimator and the estimation is more accurate close to the wall.

### 4.4. Compensator

The final stage is combining the full information controller and the estimator into the compensator. The procedure requires the estimator to run first without the control until the estimated field approaches the real flow; afterwards the control forcing is turned on. The control region is placed downstream of the estimated field and an overlap between the two strips is avoided. At the location where the actuation is active, the amplitude of the streaks is

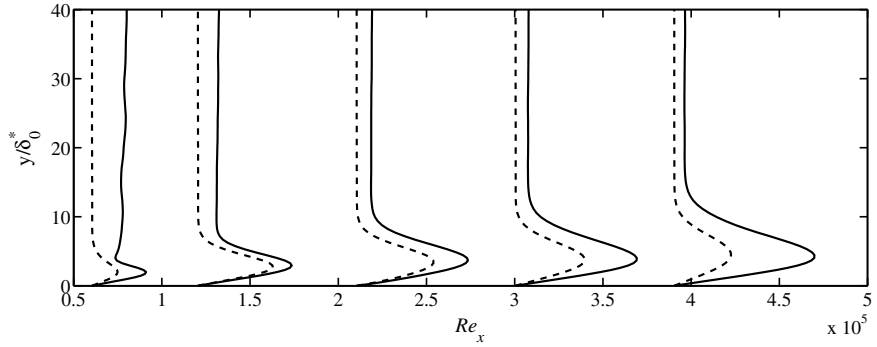


**Fig. 13.** Wall-normal profile of $u_{\mathrm{rms}}$ at different streamwise positions $Re_x = [0.6, 1.2, 2.1, 3.0, 3.9] \times 10^5$. The values of $u_{\mathrm{rms}}$ are scaled with $9.0 \times 10^5$. Real flow, ; Estimated flow, – – – –.

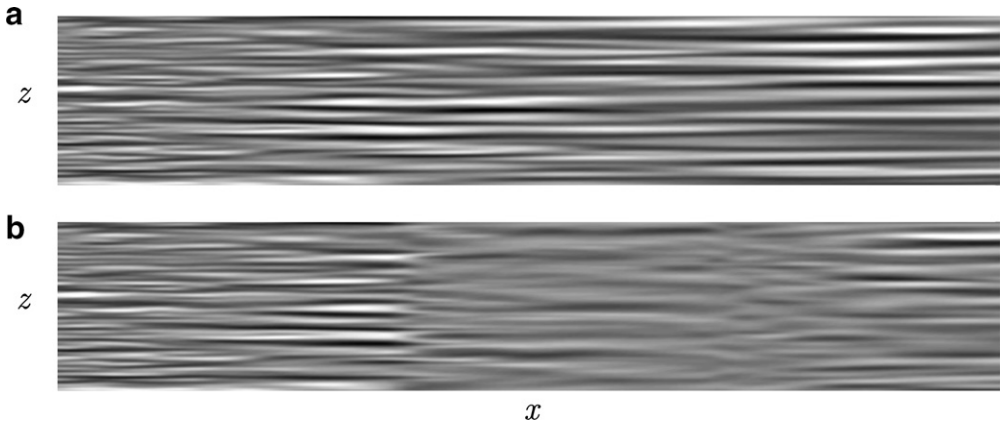


**Fig. 14.** Instantaneous streamwise velocity fields. (a): uncontrolled; and (b): controlled. Streamwise extent $Re_x = [32,000,\ 382,000]$, wall-normal distance $2\delta_0^*$, true aspect ratio.

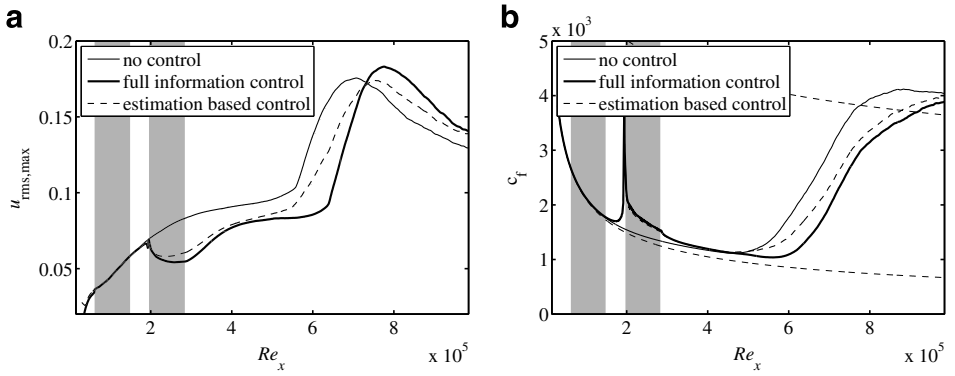


**Fig. 15.** (a): Wall-normal maximum $u_{\mathrm{rms}}$; (b): skin friction coefficient $c_{\mathrm{f}}$. No control, —; Full information control, —; Compensator, – – – –.

significantly increased. The perturbations to be controlled are further downstream, i.e. in the region where nonlinear effects are more important.

A visualisation of the controlled and uncontrolled flow field is displayed in Fig. 14 in a wall-parallel plane. The decrease of the streak amplitude in the control region is clearly visible. A turbulent spot is appearing further downstream in the uncontrolled flow while the flow is laminar when blowing/suction is applied. It can also be noticed that the control often changes an incoming high-speed streak into a low-speed region and vice versa. Further, a rapid increase in the streak amplitude is occurring after the end of the control region.

In Fig. 15a, the wall-normal maximum of the rms-value of the streamwise velocity perturbation is shown for the uncontrolled case and for both full information control and compensation. As observed by the flow visualisation in Fig. 15a, the growth of the streaks is reduced within the control region. However, downstream of the control region, velocity fluctuations continue to grow. This can be explained by the presence of the free-stream turbulence above the boundary layer that is able to induce new perturbations inside the boundary layer.

The skin friction coefficient is shown in Fig. 15b. This plot quantifies the transition delay which can be achieved in the case of boundary-layer transition induced by free-stream turbulence. The transition delay obtained without estimation corresponds approximately to the length of the control region. The delay is between $120,000\nu/U_\infty$ and corresponds to approximately 15–20% of the full length of a typical turbine blade, resulting in a reduction of the total friction drag of 5–10%. The loss of performance to be expected in the case of control based on estimation from wall measurements is not severe. Thus, a longer control region or alternatively a sequence of measurement and blowing/suction strips may lead to further delay or even prevent the transition process.

In Fig. 16, wall-normal profiles of the rms value of the streamwise velocity perturbation are shown at different streamwise stations along the plate for the three cases under consideration. The reduction of streak amplitude is evident in the control region. Note also that where blowing/suction is applied the profiles feature a double-peak structure: the lowest peak closest to the wall is due to the local effect of the actuation, while the largest peak, representing the streak, is moved away from the wall. The changeover from laminar to turbulent streaks is occurring in the region $5 \times 10^5 < Re_x < 7 \times 10^5$. The typical profiles for $u_{\mathrm{rms}}$ of a turbulent boundary layer are observed at the end of the computational domain.

The production of turbulent kinetic energy $\overline{uv}\partial U/\partial y$ with the Reynolds shear stress $\overline{uv}$, is considered to characterise the effect of the blowing/suction at the wall. The wall-normal profiles of the turbulent production at two streamwise positions are displayed in Fig. 17. It can be seen that the turbulence production increases near the wall due to the blowing and suction while it decreases farther up in the boundary layer, attaining negative values at the beginning of the control region. In the compensator a reduction over the whole profile is observed as well as a small peak near the wall.

In order to study the performance of the control for higher streak amplitudes, simulations with turbulence intensity $Tu = 4.0\%$ are also performed. Owing to the larger turbulence intensity the growth of the streaks is faster, the transition location is moved upstream and the amplitude of the streaks within the control region are further increased. Overall, the performance of the estimation is as in the case presented above, while the

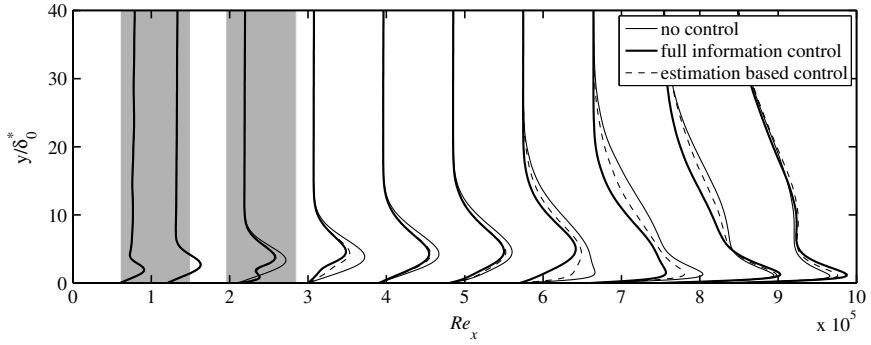


**Fig. 16.** Wall-normal profiles of $u_{\mathrm{rms}}$ at different streamwise positions $Re_x = [0.6, 1.2, 2.1, 3.0, 3.9, 4.8, 5.7, 6.6, 7.5, 8.4] \times 10^5$. The values of $u_{\mathrm{rms}}$ are scaled with $8.5 \times 10^5$. No control, —; Full information control, —; Compensator, – – – –.

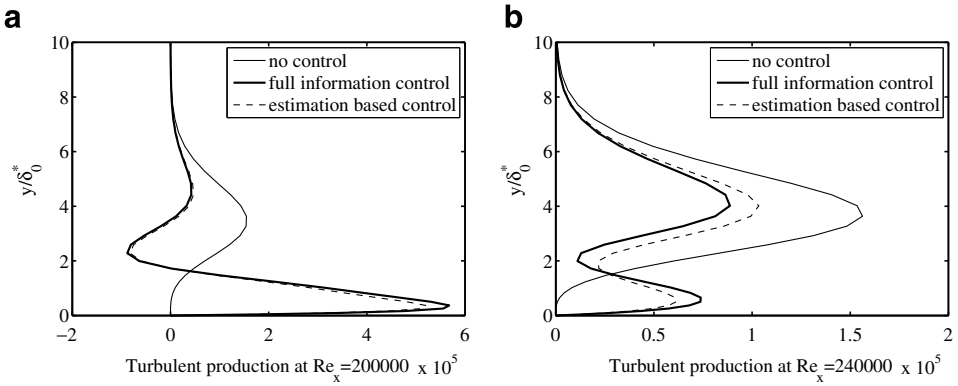


**Fig. 17.** Wall-normal profiles of turbulent production at (a) $Re_x = 2.0 \times 10^5$ and (b) $Re_x = 2.4 \times 10^5$. No control, —; Full information control, —; Compensator, – – – –.

extension of the transition delay is reduced. Even though the growth of the streaks is reduced in the control region, the regeneration downstream is more rapid at this higher free-stream turbulence levels. As shown by Barri (2006), for the control to be more effective, maybe the actuation region should be placed further upstream.

## 5. Conclusions

Numerical simulations of the transition to turbulence occurring in a flat-plate boundary-layer flow subjected to high levels of free-stream turbulence are performed. This scenario, denoted bypass transition, is characterised by the non-modal growth of streamwise elongated disturbances, so-called streaks. When these streaks reach large enough amplitudes, breakdown into turbulent spots occurs via their secondary instability. The scenario under consideration is highly intermittent in nature, i.e. streaks appear randomly in the boundary layer, and therefore large computational domains and long integration times are needed to obtain converged statistical data.

In order to reduce the computational cost, mostly large-eddy simulations are performed. The ADM-RT subgrid-scale model is shown to be particularly suited for transitional flows: it is thoroughly validated before examining the effect on the transition process. The results indicate that the details of the streak breakdown can and need to be captured by LES. The high-frequency oscillations of the elongated streaks appearing as spot precursors define the grid size on which the LES can be performed. The reduction in terms of number of degrees of freedom compared to a full DNS is of the order of 10, while the computational cost is reduced about 50 times.

Linear model-based feedback control is applied in order to delay transition, where the linear parallel Orr–Sommerfeld/Squire system is used to design the estimation and control laws. The method presented here was previously developed by Hoepffner et al. (2005); Chevalier et al., 2006; Chevalier et al., 2007a and shown to be successful in damping linear and weakly nonlinear perturbation in a variety of wall-bounded shear flows. The method is now applied to flows with highly nonlinear behaviour.

In practical situations, the full flow field is usually not accessible. The control problem is therefore combined with an estimation procedure based on wall measurements, the two wall-parallel components of the wall-shear stress and the pressure at the wall being considered here. It is found that to achieve an accurate estimation most of the confidence should be put in the shear-stress data; the pressure measurements are in fact too affected by the high-level fluctuations in the free stream.

The results presented show that the control is able to reduce the energy of the streaks, which are responsible, through their secondary instabilities, for the considered bypass-transition scenario and thus delay the whole process. The delay achieved is of order of the streamwise extent of the area where control is applied. For turbomachinery applications, this amounts to about 15–20% of the length of a typical turbine blade, resulting in a reduction of the total friction drag of 5–10%. The control performance is limited by the fast growth of the streaks just downstream of the region where blowing and suction is applied. This recovery is similar to that observed when control of turbulent flow is investigated and it can be explained by considering the action of the control in these highly disturbed flow: When blowing/suction is applied, the streamwise streaks are quenched close to the wall while the upper part of the boundary layer is less affected. As a consequence, as soon as the actuation is turned off, the streaks diffuse into the shear layer near the wall and can again be amplified. The relatively fast recovery of the streamwise streaks downstream of the control region was also observed in the recent experimental work by Lundell (2007). This author considers the same transition scenario but a different control strategy: reactive control is applied with sensors and actuators placed in a staggered manner. A more direct comparison between the linear optimal control and the experiments appears therefore relevant and it is the object of new investigations.

The streamwise streaks can be estimated from wall measurements alone; however the structures occurring in the real flow are reproduced correctly mainly in the region where the measurements are taken. Downstream of this region the estimated field gradually diverges from the real field, revealing the importance of the continuous excitation of the boundary layer by the external free-stream turbulence (Westin et al., 1998). Control based on estimation (termed compensator) is therefore less effective than full information control. For actual implementations of feedback control the estimation process needs to be improved, in particular by reducing its cost. With this aim, two directions may be followed. First, model reduction can be introduced in the estimation problem. Global modes of the flow can be used for this, as global eigenmodes (Åkervik et al., 2007) or balanced POD modes (Rowley, 2005). The model based on these two- or three-dimensional modes does not need to be linear, possibly improving the estimation performance for this type of flows. Alternatively, the relation between sensors and actuators may be deduced directly from flow measurements, relaxing the need for a flow model, as suggested, e.g. by Lundell (2007). The latter option will be the object of future work, in the context of a closer interplay between experiments and simulations.

## Acknowledgements

The authors wish to thank Mattias Chevalier, Espen Åkervik and Jérôme Hœpffner for many fruitful discussions. Computer time was provided by the Centre for Parallel Computing (PDC) at KTH, Stockholm. The present work is supported by the EOARD Grant FA8655-07-1-3053 which is gratefully acknowledged.

## References

Åkervik, E., Hoepffner, J., Ehrenstein, U., Henningson, D.S., 2007. Optimal growth, model reduction and control in a separated boundary-layer flow using global modes. J. Fluid Mech. 579, 305–314.

Andersson, P., Berggren, M., Henningson, D.S., 1999. Optimal disturbances and bypass transition in boundary layers. Phys. Fluids 11, 134–150.

Bagheri, S., Hoepffner, J., Schmid, P.J., Henningson, D.S., in press. Input–output analysis and control design applied to a linear model of spatially developing flows. Appl. Mech. Rev.

Barri, M., 2006. Optimal control of bypass transition in boundary layers. Master's Thesis, KTH Mechanics, Stockholm, Sweden.

Berggren, M., 1998. Numerical solution of a flow-control problem: vorticity reduction by dynamic boundary action. SIAM J. Sci. Comp. 19 (3), 829–860.

Bewley, T., Temam, R., Ziane, M., 2000. A general framework for robust control in fluid mechanics. Physica D 138, 360–392.

Bewley, T.R., 2001. Flow control: new challenges for a new renaissance. Prog. Aerosp. Sci. 37, 21–58.

Bewley, T.R., Moin, P., Teman, R., 2001. DNS-based predictive control of turbulence: an optimal benchmark for feedback algorithms. J. Fluid Mech. 447, 179–225.

Bewley, T.R., Protas, B., 2004. Skin friction and pressure: the 'footprints' of turbulence. Physica D 196, 28–44.

Brandt, L., 2007. Numerical studies of the instability and breakdown of a boundary-layer low-speed streak. Eur. J. Mech./B Fluids 26 (1), 64–82.

Brandt, L., Henningson, D.S., 2002. Transition of streamwise streaks in zero-pressure-gradient boundary layers. J. Fluid Mech. 472, 229–262.

Brandt, L., Henningson, D.S., 2004. Linear feedback control of perturbations developing in a boundary layer under free-stream turbulence. In: Andersson, H.I., Krogstad, P.A. (Eds.), Advances in Turbulence X, Proceedings of the 10th European Turbulence Conference, CIMNE, pp. 767–770.

Brandt, L., Schlatter, P., Henningson, D.S., 2004. Transition in boundary layers subject to free-stream turbulence. J. Fluid Mech. 517, 167–198.

Chevalier, M., Hoepffner, J., Åkervik, E., Henningson, D.S., 2007a. Linear feedback control and estimation applied to instabilities in spatially developing boundary layers. J. Fluid Mech. 588, 163–187, 167–187.

Chevalier, M., Hoepffner, J., Bewley, T.R., Henningson, D.S., 2006. State estimation in wall-bounded flow systems. Part 2. Turbulent flows. J. Fluid Mech. 552, 167–187.

Chevalier, M., Schlatter, P., Lundbladh, A., Henningson, D.S., 2007b. Simson: A pseudo-spectral solver for incompressible boundary layer flows. Technical Report KTH/MEK/TR-07/07-SE, KTH, Department of Mechanics, Stockholm.

Collis, S., Chang, Y., Kellogg, S., Prabhu, R.D., 2000. Large eddy simulation and turbulence control. AIAA Paper (2000-2564).

Farrell, B.F., Ioannou, P.J., 1996. Turbulence suspension by active control. Phys. Fluids 8 (5), 1257–1268.

Friedland, B., 1986. Control System Design: An Introduction to State-space Methods. Dover, Mineola, New York.

Grosch, C.E., Salwen, H., 1978. The continuous spectrum of the Orr–Sommerfeld equation. Part 1. The spectrum and the eigenfunctions. J. Fluid Mech. 87, 33–54.

Henningson, D.S., 1996. Comment on: Transition in shear flows. Nonlinear normality versus non-normal linearity. Phys. Fluid 8 (8), 2257–2258 (Phys. Fluids 7 (1995) 3060).

Hoepffner, J., Chevalier, M., Bewley, T.R., Henningson, D.S., 2005. State estimation in wall-bounded flow systems. Part 1. Perturbed laminar flows. J. Fluid Mech. 534, 263–294.

Högberg, M., Bewley, M., Henningson, D.S., 2003a. Relaminarization of $Re_\tau = 100$ turbulence using gain scheduling and linear state-feedback control. Phys. Fluids 15, 3572–3575.

Högberg, M., Bewley, M., Henningson, D.S., 2003c. Linear feedback control and estimation of transition in plane channel flow. J. Fluid Mech. 481, 149–175.

Högberg, M., Chevalier, M., Henningson, D.S., 2003b. Linear compensator control of a pointsource induced perturbation in a Falkner–Skan–Cooke boundary layer. Phys. Fluids 15, 2449–2452.

Högberg, M., Henningson, D.S., 2002. Linear optimal control applied to instabilities in spatially developing boundary layers. J. Fluid Mech. 470, 151–179.

Jacobs, R.G., Durbin, P.A., 2001. Simulations of bypass transition. J. Fluid Mech. 428, 185–212.

Joshi, S.S., Speyer, J.L., Kim, J., 1995. Modeling and control of two dimensional Poisuille flow. In: Proceedings of the 34th IEEE Conference on Decision and Control, pp. 921–927.

Joslin, R.D., 1998. Aircraft laminar flow control. Annu. Rev. Fluid Mech. 30, 1–29.

Joslin, R.D., Erlebacher, G., Hussaini, M.Y., 1996. Active control of instabilities in laminar boundary layers-overview and concept validation. J. Fluids Eng. 118 (3), 494–497.

Joslin, R.D., Gunzburger, M.D., Nicolaides, R.A., 1997. A self-contained automated methodology for optimal flow. AIAA J. 35 (5), 816–824.

Kailath, T., Hassibi, A.H.S.B., 2000. Linear Estimation. Prentice Hall, New Jersey.

Karamanos, G.-S., Karniadakis, G.E., 2000. A spectral vanishing viscosity method for large-eddy simulations. J. Comput. Phys. 163, 22–50.

Kim, J., Bewley, T.R., 2007. A linear systems approach to flow control. Annu. Rev. Fluid Mech. 38 (1), 383–417.

Kim, J., Lim, J., 2000. A linear process in wall-bounded turbulent shear flows. Phys. Fluids 12 (8), 1885–1888.

Landahl, M.T., 1980. A note on an algebraic instability of inviscid parallel shear flows. J. Fluid Mech. 98, 243–251.

Laurien, E., Kleiser, L., 1989. Numerical simulation of boundary-layer transition and transition control. J. Fluid Mech. 199, 403–440.

Lewis, F.L., Syrmos, V.L., 1995. Optimal Control. Wiley-Interscience, New York.

Lundbladh, A., Berlin, S., Skote, M., Hildings, C., Choi, J., Kim, J., Henningson, D.S., 1999. An efficient spectral method for simulation of incompressible flow over a flat plate. Technical Report KTH/MEK/TR-99/11-SE, KTH, Department of Mechanics, Stockholm.

Lundell, F., 2007. Reactive control of transition induced by free-stream turbulence: an experimental demonstration. J. Fluid Mech. 585, 41–71.

Mans, J., de Lange, H.C., van Steenhoven, A.A., 2007. Sinuous breakdown in a flat plate boundary layer exposed to free-stream turbulence. Phys. Fluids 19 (088101).

Matsubara, M., Alfredsson, P.H., 2001. Disturbance growth in boundary layers subjected to free stream turbulence. J. Fluid. Mech. 430, 149–168.

Metcalfe, R.W., 1994. Boundary layer control: a brief review. In: Wagner, S., Periaux, J., Hirschel, E. (Eds.), Computational Fluid Dynamics'94, Invited lectures of the Second European CFD Conference; Stuttgart, Germany. Progress in Astronautics and Aeronautics. John Wiley & Sons, pp. 52–60.

Moin, P., Bewley, T., 1994. Feedback control of turbulence. Appl. Mech. 47 (6), S3–S13 (Part 2).

Moin, P., Mahesh, K., 1998. Numerical simulation: a tool in turbulence research. Annu. Rev. Fluid Mech. 30, 539–578.

Nordström, J., Nordin, N., Henningson, D.S., 1999. The fringe region technique and the Fourier method used in the direct numerical simulation of spatially evolving viscous flows. SIAM J. Sci. Comp. 20, 1365–1393.

Reddy, S.C., Henningson, D.S., 1993. Energy growth in viscous channel flows. J. Fluid Mech. 252, 209–238.

Robinson, S.K., 1991. The kinematics of turbulent boundary layer structure. Technical Report TM 103859, NASA.

Rowley, C.W., 2005. Model reduction for fluids using balanced proper orthogonal decomposition. Int. J. Bifurc. Chaos 15 (3), 997–1013.

Schlatter, P., Stolz, S., Kleiser, L., 2004. LES of transitional flows using the approximate deconvolution model. J. Heat Fluid Flow 25 (3), 549–558.

Schlatter, P., Stolz, S., Kleiser, L., 2006a. Analysis of the SGS energy budget for deconvolution- and relaxation-based models in channel flow. In: Lamballais, E., Friedrich, R., Geurts, B.J., Métais, O. (Eds.), Direct and Large-Eddy Simulation VI. Springer, Dordrecht, The Netherlands, pp. 135–142.

Schlatter, P., Stolz, S., Kleiser, L., 2006b. LES of spatial transition in plane channel flow. J. Turbul. 7 (33), 1–24.

Schmid, P.J., Henningson, D.S., 2001. Stability and Transition in Shear Flows. Springer, New York.

Seyed, M.M., 2007. Estimation and control of bypass transition in the Blasius boundary layer. Master's Thesis, KTH Mechanics, Stockholm, Sweden.

Skogestad, S., Postlethwaite, I., 2005. Multivariable Feedback Control, second ed.. Analysis and Design Wiley, West Sussex.

Stolz, S., Adams, N.A., 1999. An approximate deconvolution procedure for large-eddy simulation. Phys. Fluids 11 (7), 1699–1701.

Stolz, S., Adams, N.A., Kleiser, L., 2001. An approximate deconvolution model for large-eddy simulation with application to incompressible wall-bounded flows. Phys. Fluids 13 (4), 997–1015.

Thomas, A.S.W., 1983. The control of boundary-layer transition using a wave-superposition principle. J. Fluid Mech. 137 (Dec.), 233–250.

Thomas, A.S.W., 1990. Active wave control of boundary-layer transition. In: Bushnell, D.M., Hefner, J.N. (Eds.), Viscous Drag Reduction in Boundary Layers, Progress in Astronautics and Aeronautics, vol. 123. American Institute of Aeronautics and Astronautics, Washington, DC.

Westin, K.J.A., Bakchinov, A.A., Kozlov, V.V., Alfredsson, P.H., 1998. Experiments on localized disturbances in a flat plate boundary layer. Part 1: the receptivity and evolution of a localized free stream disturbance. Eur. J. Mech. B Fluids 17, 823–846.